Chemical Engineering Journal 507 (2025) 160604

Contents lists available at ScienceDirect

Chemical Engineering Journal

journal homepage: www.elsevier.com/locate/cej

Octopus-inspired multichannel tactile sensor for enhanced underwater material identification

Yutao Hao [a,b,1], Yanshuo Sun [b,c,1], Jing Wen [d,1], Xiaobo Gao [b,c], Yutong Wang [e], Zhiyuan Zhu [a,*], Zhong Lin Wang [b,c,f,*], Baodong Chen [b,c,*]

[a] Chongqing Key Laboratory of Nonlinear Circuits and Intelligent Information Processing, College of Electronic and Information Engineering, Southwest University, Chongqing 400715, PR China
[b] Beijing Institute of Nanoenergy and Nanosystems, Chinese Academy of Sciences, Beijing 101400, PR China
[c] School of Nanoscience and Engineering, University of Chinese Academy of Sciences, Beijing 100049, PR China
[d] Research Institute of Technology of Shougang Group, Beijing 100043, PR China
[e] The Key Laboratory of High Temperature Electromagnetic Materials and Structure of MOE, Wuhan University of Science and Technology, Wuhan 430081, PR China
[f] Georgia Institute of Technology, Atlanta, GA 30332-0245, USA

ARTICLE INFO

Keywords:
Triboelectric nanogenerators
Bionic structure
Underwater material identification
Tactile sensing

ABSTRACT

The sustainable development of the ocean requires sensors capable of detecting objects in underwater or high humidity conditions. However, traditional sensors struggle in complex underwater environments due to signal attenuation, biofouling, and flow interference, which seriously affect their performance and reliability. Inspired by the tactile system of octopus suckers, we developed a tactile sensor that mimics the structure of octopus tentacle suckers, ingeniously harnessing triboelectric tactile receptors (TTRs) to emulate the mechanism of cephalopod-specific chemoreceptors (CRs), aiming to address the challenging problem of underwater object recognition. Additionally, the superhydrophobic treatment enhances the microstructure of the sensor surface, effectively mitigating environmental interference and improving underwater performance, leading to a 67 % increase in voltage output, a sensitivity of 0.195 V kPa^{-1}, and a remarkable response time of 85 ms. Most importantly, we have constructed an underwater material identification system (UMIS) to achieve 98 % accuracy by integrating machine learning, which enables precise identification and quantitative sensing of underwater objects, and offering novel insights and directions for the intelligence and autonomy of underwater robots.

1. Introduction

With the development of economy and technology, electronic products have been manufactured rapidly, we are now in a resource-dependent society. However, the fast growth has further exacerbated the depletion of resources and environmental pollution, especially in the ocean [1]. Due to the scarcity of oxygen in seawater and the improper discharge of garbage, substantial obstacles arise in marine environment health and seabed development, making the exploration of the ocean's vast resources increasingly difficult [2–4].

In order to solve the above problems, it is essential to accurately detect and identify various objects in the underwater environment [5,6]. However, underwater object recognition remains challenging owing to the intricate underwater conditions and low visibility [7–9]. Therefore, the development of intelligent sensing technologies that embody both environmental friendliness and high sensitivity is paramount importance [10–13]. Up to now, various underwater detection methods, such as the vision imaging [14], thermal sensitivity principle [15], ultrasonic and tactile scheme [16], have been utilized in different underwater applications. Despite great advances in underwater material identification, but always with limitations. Specifically, Visual scheme suffers from poor image quality given the light scattering and low visibility. For thermal detection, the rapid attenuation of thermal signals in water hinders the detection of temperature gradients. In addition, ultrasonic technology is susceptible to underwater noise and the multi-channel effect, resulting in echo delays and superposition that undermine the accuracy of material identification. Meanwhile, tactile sensors face challenges associated with the charge shielding effect, which reduces

* Corresponding authors.
E-mail addresses: zyuanzhu@swu.edu.cn (Z. Zhu), zlwang@gatech.edu (Z.L. Wang), chenbaodong@binn.cas.cn (B. Chen).
[1] Y. H., Y. S. and J. W., these authors contributed equally to this work.

https://doi.org/10.1016/j.cej.2025.160604
Received 23 September 2024; Received in revised form 1 December 2024; Accepted 11 February 2025
Available online 12 February 2025
1385-8947/

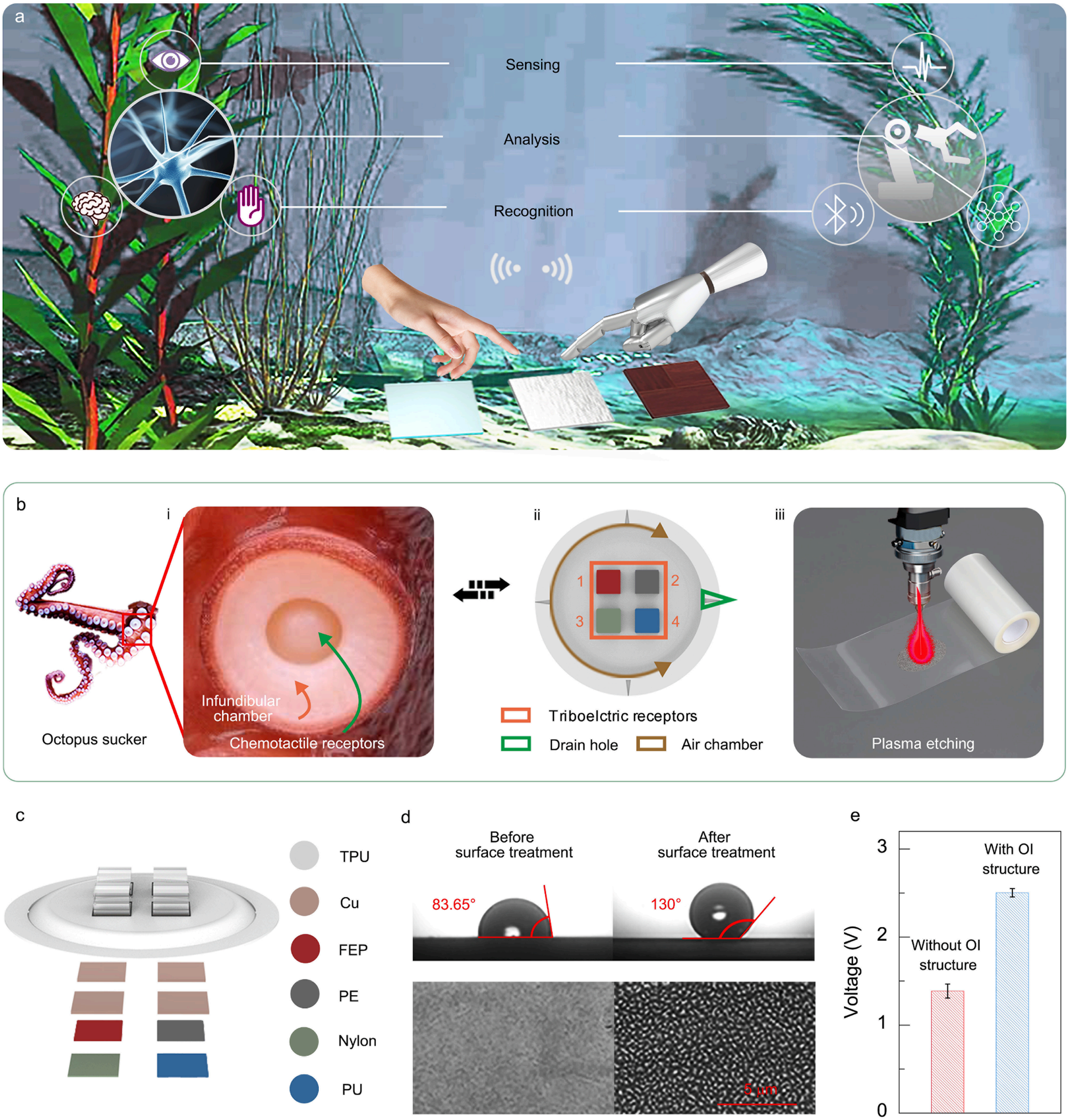

Fig. 1. Structure design and schematic of OI-TENG. (a) Schematic diagram of the underwater material identification process of the OI-TENG. (b) Schematic diagram of biomimetic sucker structure information and function of each region. (c) Exploded view of structure design of the OI-TENG. (d) The surface treatment of triboelectric receptor SEM images and contact angle of receptor surface before and after surface treatment. (e) The output performance of the device with and without OI structure.

the recognition ability of the sensor. Therefore, the design of a multi-channel tactile identification sensor remains unaffected characteristic by underwater environments, which is crucial for resource exploration and material identification [17–19], contributing to improved intelligence and operational efficiency in underwater sensing devices [20–22].

Bionic tactile sensing emerges as a novel trend in material identification [23–25], relying on widely distributed nervous systems to detect objects via chemotactile receptors, which not only sense force and shape [26], but also detect the material of the object, while effectively filtering out most external interference [27–29]. In the field of sensors, triboelectric nanogenerator (TENG) have a similar mechanism to convert mechanical signals into electrical signals acceptable to triboelectric receptors [30], based on triboelectrification and electrostatic coupling effects [31,32]. Due to its high sensitivity, real-time response, flexibility and signal stability, it has a significant advantages in the field of sensors [33,34], and has been widely applied in physiological information monitoring [35,36], energy harvesting sensing [37], sport analysis and alert [38]. However, it is susceptible to the environmental factors,

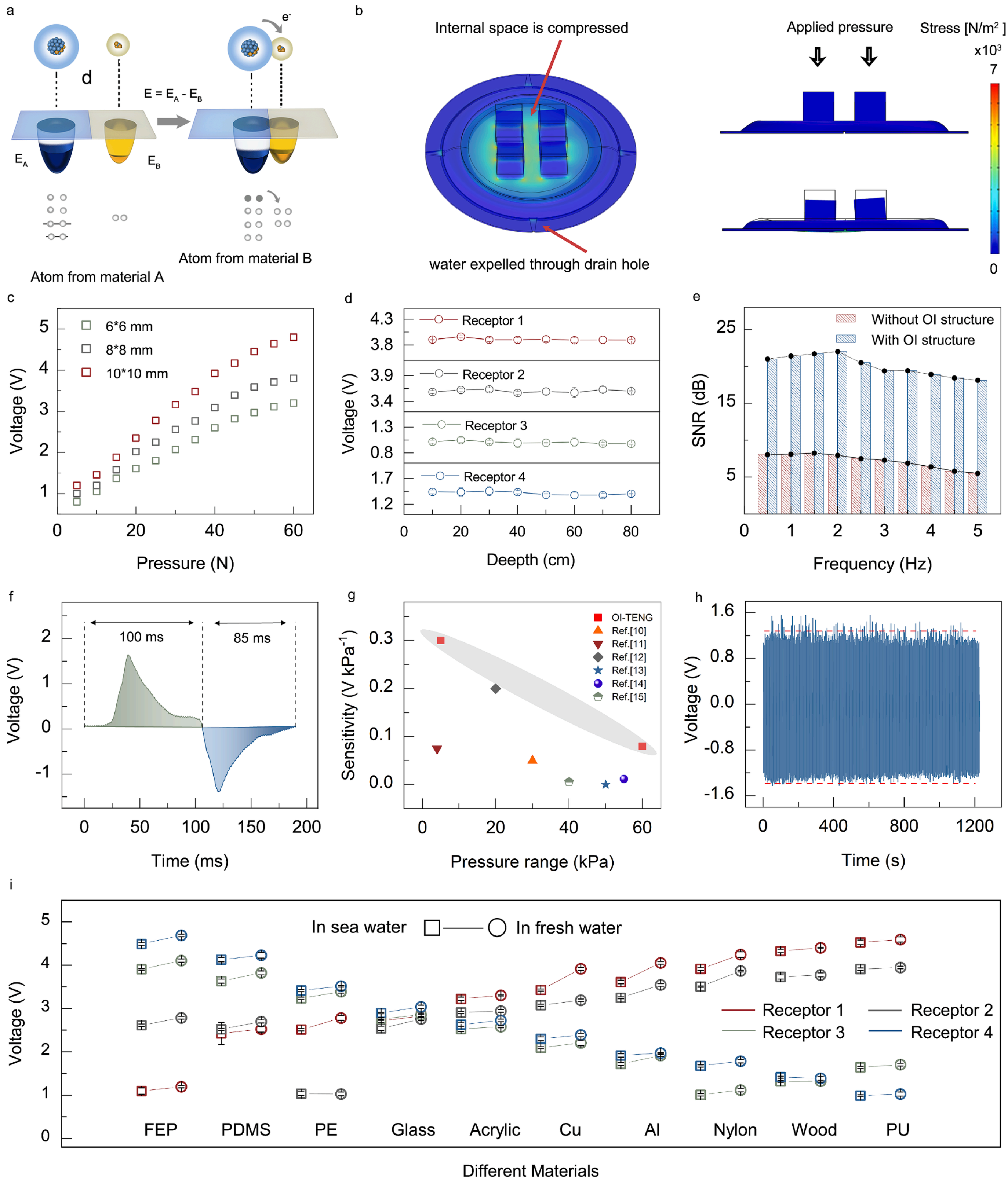

Fig. 2. Mechanism of triboelectric sensing and sensor performance characterization. (a) The fundamental principle of triboelectricity explained by the overlapping electron cloud model. (b) 3D illustration of the working mechanisms of OI-TENG and strain simulation in the process for detecting objects. (c) Output voltage of the receptor to contact materials with different sizes. (d) The output performance of the device detecting the underwater object in different water depth. (e) The change in SNR of sensor with OI structure and without OI structure. (f) Response time and recovery time of the sensing signals. (g) Comparison of the sensitivity with other sensors. (h) Mechanical durability characterization of the TENG with over 3500 continuous working cycles. (i) The sensing signal of OI-TENG in different water environment.

especially humidity and water [39–41]. According to the above principles, a signal analysis system was established to interpret the distinct electrical signals generated by different materials. By utilizing varied triboelectric receptors, it is possible to comprehensively analyze material types based on the various signal characteristics. While optimizing the triboelectric receptors to diminish the impact from the environmental factors. For quantifiable tactile response and material analysis [37,42].

Here, we develop a multichannel tactile sensing system inspired by octopus tentacles for real-time underwater materials identification based on triboelectric nanogenerator (OI-TENG). The sucker structure of OI-TENG mimics the tentacles of octopus, utilizing several typical materials placed at different positions in the triboelectric sequence as receptors [43], with superhydrophobic treatment on surface to receive the charges generated upon contact with materials underwater [41]. Even in different external environments, the proportion of signal remains consistent in a certain range. Through comprehensive multi-channel tactile analysis, the relevant information about the object material can be obtained. Moreover, to further reduce environmental interference and improve the identification accuracy, an underwater material identification system (UMIS) was established, which employs machine learning algorithms to validate and classify signals received via wireless communication module, and transmits to the terminal display in real time, achieving a material identification accuracy up to 98 %. The bionic tactile identification system is characterized by simple structure, high sensitivity, and low susceptibility to underwater environment interference. The OI-TENG not only holds promise for applications in marine pollution detection and salvage rescue, but also bring a trustworthy strategy for underwater material analysis.

2. Results and discussion

2.1. Design and integration of the bioinspired tactile sensor

Cephalopods, represented by octopus, have a huge distributed nervous system that enable advanced sensations such as touch and taste. Octopuses have evolved specialized CRs on the suckers of their arms, which are used to catch prey and explore unknown environments in the ocean. Inspired by the information transmission between object and receptors, the OI-TENG employs a bionic design, which can be integrated with robotic arm for building a tactile perception system of underwater material identification. Fig. 1a shows a conceptual schematic illustration comparing object recognition by organisms and triboelectric sensors. Both systems own the common is to analyze and identify the signals received by receptors based on neural network. When the octopus touches an object, the infundibular chamber on the sucker contracts, to create a vacuum environment inside, and the specific CRs receive the corresponding ligand and determine whether it is prey (Fig. 1b(i)). The tactile sensing function of octopus tentacles was simulated based on this characteristic. Due to the different ability of materials to attract charges, when various materials contact the triboelectric receptor, the voltage generated from each receptor is collected which can realize the object material identification through analyzing the instantaneous pulse signal. The bionic structure is shown in Fig. 1b (ii), when in contact with the object underwater, the water is quickly drained by the surrounding drain holes under the external force, creating a vacuum in the air chamber to minimize the external interference as much as possible. Due to the OI-TENG use the materials TPU, which own the characteristic of low compression modulus, initial deformation can be triggered by tiny forces, makes it easier to fit the sample surface. Meanwhile, the device has the characteristics of elastomer material, the compression modulus further decreases with the increases temperature, resulting in better contact with the sample (Fig. S1). The overall design is not only simple in structure and small in size, but also optimizes the stability of the electrical signal upon contact, through plasma etching to process the surface of the receptors (Fig. 1b (iii)). OI-TENG tactile sensor consists of four triboelectric receptors and a compressible air chamber. An exploded view of the device can demonstrate the structure clearly shown in Fig. 1c. Four acrylic columns serve as supports and links, with four materials occupying different positions in the triboelectric sequence and attached to the copper substrate as triboelectric receptors. An air chamber made of thermoplastic polyurethane (TPU) by 3D printing process. Fig. 1d shows the contact angle and scanning electron microscopy (SEM) images of FEP film (receptor 1) before and after surface treatment. It can be observed that the surface of the film without ICP (inductively coupled plasma) treatment is relatively rough, with a contact angle of 83.65°. However, after 40 s of ICP treatment, spines and holes appeared in SEM image, indicating the formation of a nanoforest similar to the surface of lotus leaf, and the contact angle also increases to 130°, making the film nearly superhydrophobic, which means the triboelectric receptors less susceptible in underwater environment. The corresponding ICP etching result with different times of each receptor have been demonstrated as new Fig. S2. To further verify this conclusion, the output performance of the OI-TENG with and without surface treatment was measured under different pressures. The curve variation of voltage with pressure changing is shown in Fig. S3. In the applied force range of 5–60 N, the output performance of the surface treated OI-TENG was higher than non-surface treated OI-TENG. Compared to the sensor without such structure, the output performance of this device was significantly improved due to the reduced charge loss (Fig. 1e). The corresponding voltage waveforms and amplitudes are shown in Fig. S4. During the experimental period, a thin film sample was selected and fixed it on a rigid acrylic substrate. This could ignore the impact of inconsistent contact on receptors caused by different mechanical modulus. These results demonstrate that the structure effectively shields the interference from the complex underwater environment.

2.2. Sensing mechanism and signal characteristics analysis

Extensive evidence has confirmed that contact electrification between two solids is primarily caused by electron transfer. Theoretically, triboelectric sensors can identify any object through contact electrification and charge transfer. Fig. 2a illustrates this principle through an overlapping electron cloud model. Before contact, the two materials possess independent electron clouds, with potential tightly binding electrons to specific orbits, preventing electron transfer. When the materials come into contact, the electron clouds of the contacting atoms overlap significantly, leading to the formation of new bonds. This phenomenon reduces the barrier between atoms, causing electrons to move towards the lower potential of atom. This process shifts from an initial single-well potential to an asymmetric double-well potential. The electron cloud states of various materials are different, resulting in unique electrical signals during contact, which enables material identification. Furthermore, we discuss the working principle of OI-TENG to better analyze triboelectric signal characteristics. The detection of unknown objects by the sensor is based on the single electrode mode (Fig. S5). When the two materials are separate, they are in a state of charge balance (Fig. S5(i)). As the sensor gradually approaches the object, depending on the attraction of the material to the electrons (in the case of FEP), the negative charge accumulates on the surface of the FEP, repelling electrons toward the ground (Fig. S5 (ii)). The potential reaches maximum value when in complete contact (Fig. S5 (iii)). As the sensor separates from the object, electrons flow back until the two materials are completely separated, a new charge balance is reached (Fig. S5 (iv)). A 3D schematic illustration demonstrates the operating state of the OI-TENG, when the device deformed by external force, the internal water is expelled through the drain holes. The air chamber is in a vacuum state as the device adheres to the object, triboelectric receptors contact the object and generate signals. The corresponding sectional stress distribution can be obtained through COMSOL finite element analysis, which proves the stability and feasibility of the

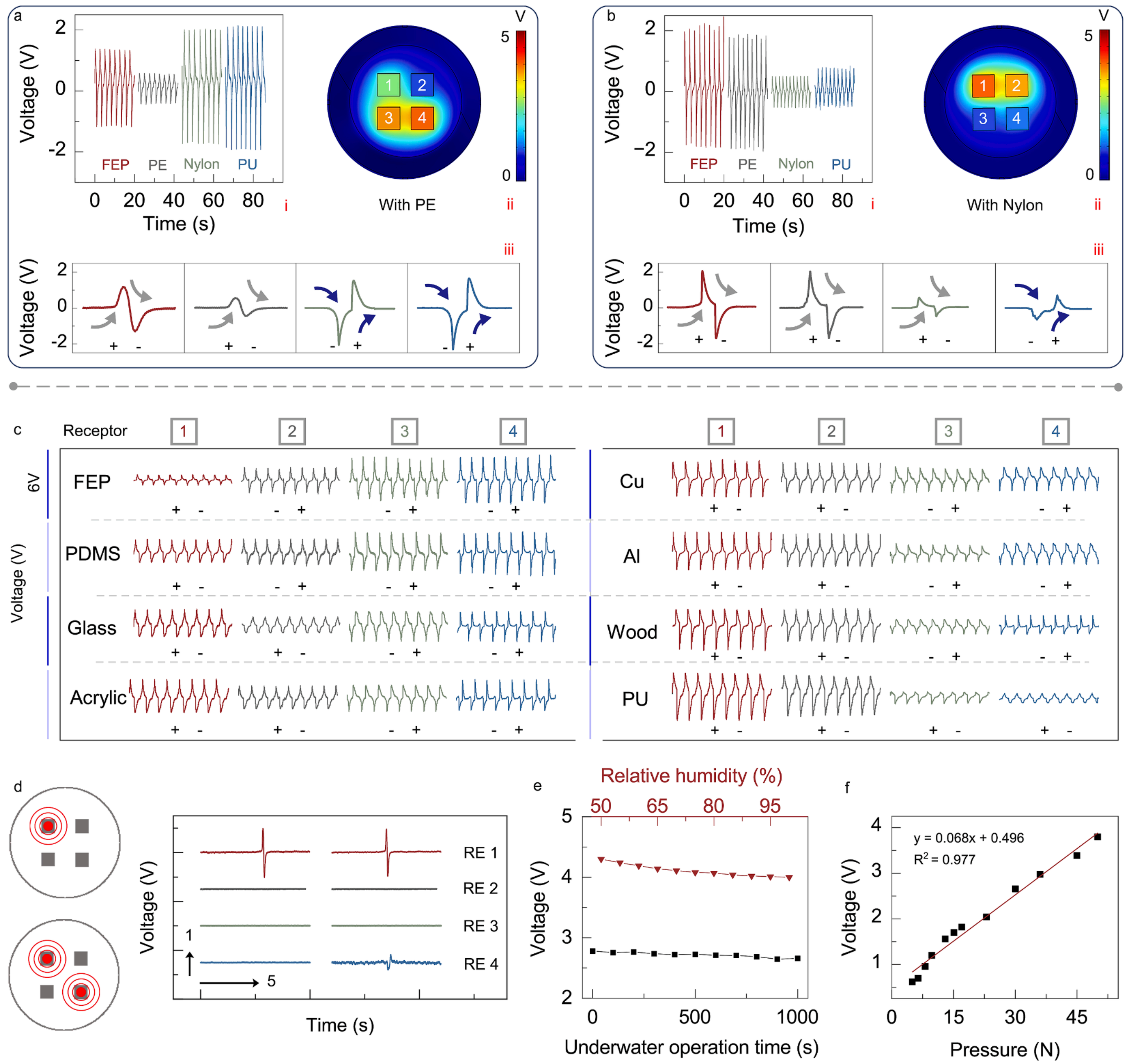

Fig. 3. Sensing characteristics analysis and material type identification. (a) The sensing signals of OI-TENG identify the PE film, four-channel potential simulation diagram and corresponding detailed output waveforms. (b) Sensing signals of OI-TENG identify the Nylon film, four-channel potential simulation diagram and corresponding detailed output waveforms. (c) Sensing characteristic of the triboelectric receptor to identify the various material of FEP, PDMS, Glass, Acrylic, Cu, Al, Wood, PU. (d) The influence between different detectors when identifying objects. (e) Output performance of OI-TENG in different humidity conditions and underwater operation times. (f) Relationship between the output voltage of OI-TENG and external pressure, and its linear fitting results (5–50 N).

structure (Fig. 2b). Considering that the identification process always occurs in open environments with dynamic effects, exploring the optimal structure and operating conditions for the OI-TENG is essential. Fig. 2c shows different sizes of the triboelectric receptor under various pressure. With the larger triboelectric receptor area, the output signal also increases, indicating that a larger contact area results in better signal. Additionally, greater external force can further optimize contact by increasing the effective contact area. However, in the practical experiment, some test sample with limited size, larger contact area may lead to insufficient contact at the edge of the receptor, which effects the accuracy of the data. After comprehensive comparation, the receptor size of 8*8mm was selected. Fig. 2d describes the output of each triboelectric receptor at different depth. The output voltage does not change significantly with increasing depth, indicating that the device ability of water pressure resistance. And the output of the device does not change with the various temperature (Fig. S6). Fig. S7 compares the output performance of devices with and without OI structure at various depths. The device without OI structure experiences more effects than OI-TENG as increasing depth. Which further confirms the potential for marine applications. To study the sensing characteristics of the OI-TENG, the signal–noise ratio (SNR) under different frequencies was analyzed. As shown in Fig. 2e, within the working frequency range of 0.5–5 Hz, SNR increases as the frequency decrease, regardless of whether the device has an OI structure, with the maximum value of 22 proves the low frequency signal stability of the OI-TENG as tactile sensor. With the fast response time of 85 ms, the triboelectric sensor can accurately recognize the

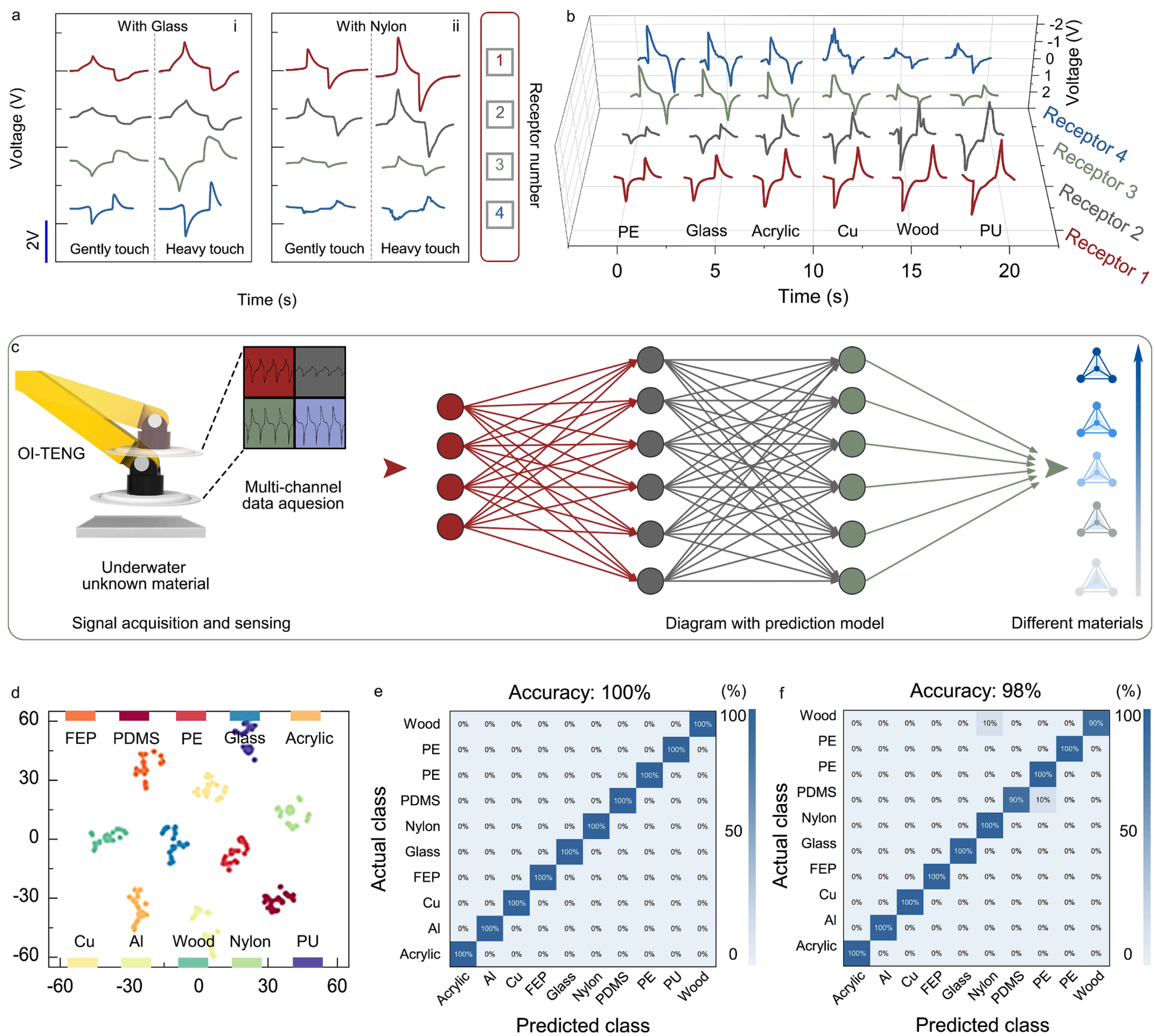

Fig. 4. Accuracy enhanced model for material identification based on machine learning. (a) Recognition results of glass and nylon film under different applied forces. (b) 3D plots of the OI-TENG underwater outputs corresponding to six random unknown materials. (c) OI-TENG schematic diagram of collecting signals from underwater materials and conceptual diagram of the machine learning training process. (d) t-SNE dimension reduction analysis of different material clusters. (e) Confusion matrix of the training set (accuracy of 100%). (f) Confusion matrix of the prediction set (accuracy of 98%).

object even at rapid contact (Fig. 2f). The sensor is designed to operate in complex environments, demonstrating high sensitivity and ultra-wide pressure bandwidth. Which is superior to other triboelectric sensors reported in the literature (Fig. 2g) [44–49], making it particularly well-suited for handling various conditions. Subsequently, the long-term stability of the OI-TENG was investigated, after more than 3500 testing cycles, the voltage maintained a consistent amplitude without obvious attenuation, proving the stability of the OI-TENG in marine detection (Fig. 2h). In order to compare the performance of the OI-TENG in different water environments and analyze the relationship between various material and the electrical signals of the triboelectric receptors, ten materials were selected for identification testing. Each sample was tested by receptors in both fresh water and seawater, connecting the two symbols of sample with short line to clearly distinguish the group. Receptor 1 and 2 with strong electronegativity, exhibit an upward trend in output, while receptor 3 and 4 with lower electronegativity show a downward trend. Which is aligns with the principle that materials with significant differences in triboelectric sequence transfer more electrons. It was also observed that the output of device in freshwater generally outperformed its output in seawater. This could be due to the presence of minerals and salts in seawater, which may prevent complete elimination the adhesion of water droplets during underwater detection. The residual electrolyte left on the surface can shield the charge on the triboelectric receptors, reducing the electrostatic induction and overall electrical output (Fig. 2i).

2.3. Signal characteristics analysis and sensing performance

According to the above work, we employed the optimized OI-TENG for material identification through tactile sensing. The materials of four triboelectric receptors are FEP, PE, Nylon and PU respectively, which based on their descending order of electronegativity. The signals collected from the integrated receptors can be cross-verified from multidimensional characteristics, significantly improving identification accuracy. Various test materials were selected to investigate the performance of the sensor. Fig. 3a shows the test of sensor on PE, revealing the reason for higher output performance for Nylon and PU, which is attributed to stronger electronegativity of PE compared to these materials. While the output of FEP was lower due to the similar electronegativity to PE, resulting in minimal output when PE is used as both the receptor and test material because the electron affinities are the same (Fig. 3a(i)). The corresponding simulation diagram provides a sensitive and salient visual potential distribution image, also confirm this result (Fig. 3a(ii)). The specific waveform detected is shown in Fig. 3a(iii), producing a waveform similar to a sine wave which contains a lot of information. When the triboelectric receptor is in contact with object, if the receptor material has stronger electronegativity than the test material, the voltage signal will show a trend of initially rising and then falling. Here, the symbol "+" represents the rising trend and the symbol "-" represents the falling trend. Conversely, the receptor material has lower electronegativity, the waveform will exhibit the opposite pattern. Based on this identification strategy, the data correctness and accuracy when testing Nylon can be verified. Due to the high electronegativity of FEP and PE, output performance is relatively high, with the waveform exhibiting an initial rising and then falling trend, denoted as "+ and −". Meanwhile, the electronegativity of PU is slightly lower than Nylon, resulting in lower output performance and an inverse waveform pattern "- and +". In particular, when receptor 3 contacts Nylon, the signal first rises and then falls, it can be concluded that the signal trend of "+ and −" is generated when tow same materials come into contact. The consistency between the detected signal amplitude and the simulated results both validates the accuracy of the result (Fig. 3b). This conclusion is drawn based on the relative positions of the materials within the triboelectric sequence, and the applicability of the sensor can be further extended to a variety of common materials, including Fluorinated Ethylene Propylene (FEP), Polydimethylsiloxane (PDMS), Glass, acrylic, Cu, Al, Wood and polyurethane (PU). Fig. 3c illustrates the unique amplitude and waveform trend of each receptor generated by OI-TENG when detecting the above materials. While the signal fluctuates within a certain range due to different external environment, the relative relationship between the receptors remains consistent. In addition to interference from touch pressure and contact area, the independence of signals in different receptors also influences sensor accuracy. To test whether different receptors interfere with each other (Fig. 3d). We observed that when receptor 1 receives an external stimulus, an output voltage about 2 V is generated, while receptors 2 to 4 show no significant fluctuations. As shown in Fig. S8, each receptor was tested individually and demonstrated excellent independence. When an additional stimulus is applied to receptor 4, adjacent receptor 2 and 3 exhibited stability similarly, indicating that the OI-TENG effectively minimizes potential interference from tactile stimuli on other receptors. This further validates that each receptor not only possesses high sensitivity but also exhibits strong anti-interference performance. Humidity and underwater environments are critical factors affecting output performance. In order to verify the stability of the OI-TENG, the performance of device was tested under various relative humidity and different underwater operation time. When the applied pressure is 10 kPa, the output performance slightly decreased from 4.3 V at 50 % relative humidity to 4 V at 100 % relative humidity, attributed to a decrease in charge density. The sensor operates continuously under the lower voltage, attributed to water interfering with electron transfer at the interface. (Fig. 3e). However, the sensitivity remains above 0.35 V kPa^{-1}, by collecting and optimizing the parameters, we can further calibrate the recognition ability of the sensor. When the sample reached the dew point temperature, dew is appeared on the surface of the sample, which simulates the droplets adhering to it. We investigated the sensitivity of the sensor in this situation, it can be seen that the dew point temperature is calculated according to the relative humidity, and the sensor sensitivity remains at about 0.28, which further proves the effectiveness of the operational mechanism (Fig. S9). When the OI-TENG is operating underwater the output performance remains stable, the surface microstructure and long-term stability are described in Fig. S10. Four receptors operate continuously within 3000 cycles without any obvious fluctuation on the signal, and surface microstructure did not change. demonstrating the strong environmental adaptability. Fig. 3f shows the voltage response under different pressures range, revealing a positive correlation. In the low-pressure range (< 50 N), the OI-TENG illustrates a strong linear response. However, in the high-pressure range (50–160 N), the effective contact area no longer increases linearly with increasing pressure, reaching a maximum of 7.4 V at 160 N (Fig. S11). Demonstrates the ability of OI-TENG to operate under extreme conditions.

2.4. Machine learning supported material identification system

By evaluating the feedback of triboelectric receptors under various touch conditions, the consistency of recognition by the OI-TENG across different external pressures was assessed by detecting materials through gentle and heavy touches respectively. When in contact with glass (Fig. 4a(i)), the receptors exhibited the same signal waveform trend as in Fig. 3c. The overall amplitude of the signal under heavy pressure is larger than under gentle touch, but the increase was approximately proportional. The same result can be found when testing Nylon (Fig. 4a (ii)). The signal obtained by heavy touch is proportional to the gentle touch, due to the larger effective contact area. Even under heavy pressure, the signals remain clear and undistorted, proving that the water has been drained by the sucker structure. These results further support the stability of the sensor in tactile recognition processes. To assess the performance of the sensor underwater, six materials were randomly selected for testing. The receptor array exhibits different trend of waveform and varying voltage amplitude (Fig. 4b). Specific materials could be identified through their unique waveforms and corresponding output. These results demonstrate the ability of the triboelectric receptor to identify material types based on triboelectric signal characteristics. Machine learning has been proven to be an effective auxiliary tool to improve recognition accuracy, which can automatically extract and process features from existing data. Before model training, 120 voltage signals were collected for each material to serve as samples, which were randomly divided into training dataset and test dataset. A convolutional neural network (CNN) was employed to analyze and identify the multidimensional data. The CNN can automatically extract features layer by layer from input signals to predict multiple response variables. In this study, various features of the data that have the greatest impact on the accuracy of machine learning predictions were selected, including absolute value of amplitude, numerical order and contact peak/valley to train the model. As the amount of training data increases, the machine learning model gradually approaches the true value (Fig. 4c). To enhance the visualization of data prediction and classification, the t-Distributed Stochastic Neighbor Embedding (t-SNE) algorithm was used for nonlinear dimensionality reduction of the data, representing the similarity between the samples. Through four-channel data acquisition, the clustering of samples is clearly observed, with sample points of each material clustered together. Although some data points overlapped the other, the clustering of data points remained distinguishable with obvious boundaries. This demonstrates the excellent classification performance of the model and proves the validity of the prediction (Fig. 4d). After extensive training, the CNN-based model reached a 100 % accuracy in identifying 10 different materials, with a 98 % accuracy on the prediction set, as shown in the confusion matrix (Fig. 4e-f). This effectively minimizing overfitting and demonstrating high generalization capabilities. The results confirm the potential of the prediction model to improve the accuracy and reliability of material identification, representing a crucial advancement for the development of underwater tactile sensing technology.

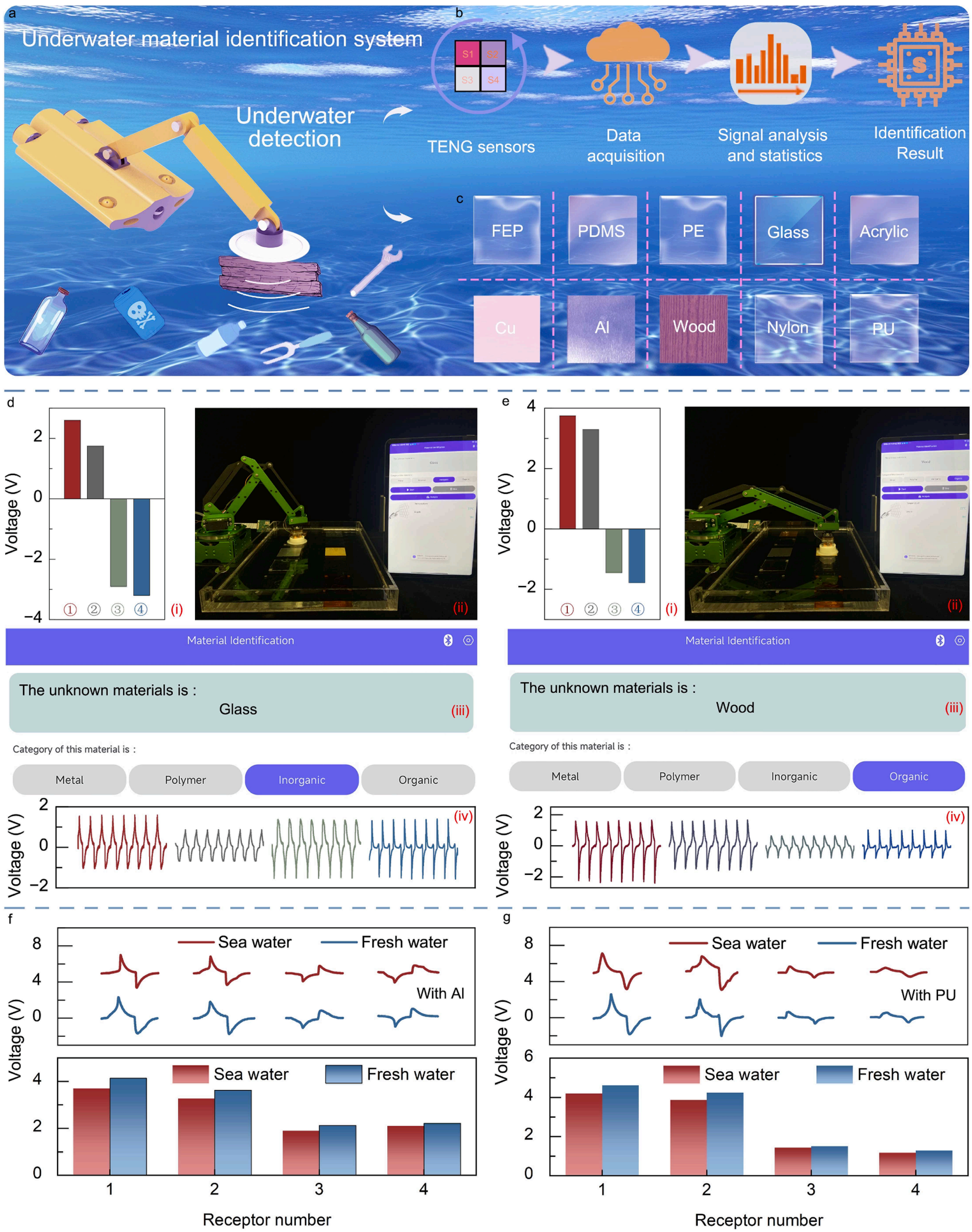

Fig. 5. Demonstration of intelligent detection system for underwater material identification through OI-TENG. (a) Schematic illustration of the OI-TENG application scenario. (b) Concept of the OI-TENG involved in an underwater unknown materials identification system. (c) Photographs of ten sorts test materials. (d-e) The voltage performance and signal characteristic of OI-TENG when identified glass and wood. The results were displayed on the wireless terminal. (f-g) The material of Al and PU detection period waveform of OI-TENG in different water environment (freshwater and sea water) and corresponding output performance.

2.5. Tactile sensing of various situation with underwater material identification system

To effectively demonstrate the performance of the OI-TENG in underwater environments, the device can be integrated into robotic arms or underwater robots, and the information was transmitted back to the terminal in real time through a wireless communication module (Fig. 5a). We developed an UMIS based on the OI-TENG to improve the accuracy and practicability of material identification as depicted in Fig. 5b. When the triboelectric receptors detect an object, the signal is calculated and analyzed simultaneously based on the preset parameters through multi-channel data acquisition, and the result is displayed on the terminal device in real time. As shown in Fig. 5c, we selected ten materials: FEP, PDMS, PE, Glass, Acrylic, Cu, Al, Wood, Nylon and PU to validate the feasibility of the UMIS. It is worth noting that these materials are difficult to distinguish completely through human touch. Fig. 5d demonstrates the real-environmental application of underwater material identification. The detection data is exhibited in Fig. 5d(i), where the positive value represents the "+ −" trend, and the negative value represents the "- +" trend of voltage signal. The triboelectric sequence of the material was identified between PE and Nylon, according to the correlation of voltage amplitude, the material was identified as glass. The corresponding test scenario and identification result are shown in Fig. 5d (ii) and (iii), while the Fig. 5d (iv) is the corresponding real-time voltage data. Fig. 5e shows the data of wood detection and the results were displayed on the terminal interface. Meanwhile, the category of material was classified according to preset parameters. Movie S1 demonstrates the UMIS based OI-TENG is continuously identifies multiple objects and obtaining results in real-time, proving the good accuracy and timeliness performance. Meanwhile, it can be seen that bubbles are generated during the test, the air and water inside are expelled, which indicates that the inside of the structure has reached an airtight state, the effectiveness of the device operating mechanism has been further verified. Fig. 5 f-g show the results of OI-TENG detecting materials in seawater and fresh water respectively, the data reveals that the same material was distinguished identified in different water environments. According to the previous signal characteristics, it can be identified that Fig. 5f is Al and Fig. 5g is PU. Although the signal amplitude is different, the other characteristics and proportions of the signal remain consistent, the identification results were not affected by the environment. The process of simulating tactile perception in different water environment is shown in detail in Movie S2.

3. Conclusion

In this work, we developed a bionic tactile sensor for material identification in underwater environments. Benefit from flexible sucker structure and optimized triboelectric receptor of OI-TENG, the device effectively eliminates underwater interference and identify objects material in various complex environments. The device demonstrates excellent performance as a sensor, which possesses an average sensitivity of 0.195 V kPa^{-1}, durability of over 3500 testing cycles and the rapid response time of 85 ms. Utilizing the machine learning algorithm established a CNN-based model to analyzed and identify signals from different materials in diverse environments by optimized algorithm, with an accuracy of 98 %. We also constructed the UMIS to visually verify results in real-time by analyzing the signal characteristics, achieving high integration and accuracy, exceeding human capabilities in materials identification through the integration of multiple perceptions. Taking these compelling advantages into account, the UMIS system holds significant potential for applications in underbed exploration, search and rescue, with important guidance for the development of intelligent sensing and bionic design in the next stage.

4. Experimental section

4.1. Fabrication of the OI-TENG: The bionic tactile sensor is composed of two main parts.

A flexible arc-shaped sucker which can adsorb on the object, use the TPU material with Shore hardness of 70 A. There are four square holes of 8*8 mm at the top integrating the receptors. 54 mm diameter in the bottom and 5 mm in height, and four drain holes evenly distributed at the bottom to expel water. Subsequently, four acrylic rods with a contact area of 8*8 are used as triboelectric receptors covered with Cu electrodes of the same size. Four different materials (FEP, PE, Nylon, PU) are adhered to the electrode, the film cover all areas of the copper electrode to avoid electrical interference and chemical corrosion caused by the underwater environment to the triboelectric receptor.

4.2. Characterization and measurement

ICP reactive ion etching (SENTECH/SI-500) was applied to fabricate nanostructures on the receptor material surface. The images of the treated receptor surface were obtained using a SEM (HITACHI SU8020). The contact angle of the film was measured by CA100C from Shanghai INNUO. The electric signal of the OI-TENG in various parameters were tested by a programmable electrometer (Keithley Instruments model 6514). A linear motor (Linmot E1100) was applied to drive the OI-TENG under different parameters. The hardness of TPU was characterized by shore hardness tester (LX-TECLOCK GS-706 N). The data and graph were processed by using Origin 2021.

CRediT authorship contribution statement

Yutao Hao: Writing – original draft, Methodology, Data curation. **Yanshuo Sun:** Visualization, Investigation. **Jing Wen:** Formal analysis. **Xiaobo Gao:** Validation. **Yutong Wang:** Formal analysis. **Zhiyuan Zhu:** Supervision, Investigation. **Zhong Lin Wang:** Writing – review & editing, Supervision, Resources, Conceptualization. **Baodong Chen:** Writing – review & editing, Funding acquisition.

Declaration of competing interest

The authors declare that they have no known competing financial interests or personal relationships that could have appeared to influence the work reported in this paper.

Acknowledgments

Y. H., Y. S. and J. W. contributed equally to this work. This work is supported by The National Key Research and Development Program of China (Grant No. 2023YFB2604600). This work is supported by Key Laboratory of High Temperature Electromagnetic Materials and Structure of MOE, Wuhan University of Science and Technology, Wuhan 430081, PR China (Grant No. KB202409).

Appendix A. Supplementary data

Supplementary data to this article can be found online at https://doi.org/10.1016/j.cej.2025.160604.

Data availability

No data was used for the research described in the article.

References

[1] J.R. Jambeck, R. Geyer, C. Wilcox, T.R. Siegler, M. Perryman, A. Andrady, R. Narayan, K.L. Law, Marine pollution plastic waste inputs from land into the ocean, Science 347 (2015) 768–771, https://doi.org/10.1126/science.1260352.

[2] P. Xu, J. Zheng, J. Liu, X. Liu, X. Wang, S. Wang, T. Guan, X. Fu, M. Xu, G. Xie, Z. L. Wang, Deep-learning-assisted underwater 3D tactile tensegrity, Research 6 (2023) 0062, https://doi.org/10.34133/research.0062.

[3] P. Xu, J. Liu, B. Liu, Y. Li, H. Jin, Z. Mu, T. Guan, G. Xie, H. Wang, M. Xu, Deep-learning-assisted triboelectric whisker for near field perception and online state estimation of underwater vehicle, Nano Energy 129 (2024) 110011, https://doi.org/10.1016/j.nanoen.2024.110011.

[4] S. Sundaram, P. Kellnhofer, Y. Li, J.-Y. Zhu, A. Torralba, W. Matusik, Learning the signatures of the human grasp using a scalable tactile glove, Nature 569 (2019) 698–702, https://doi.org/10.1038/s41586-019-1234-z.

[5] Y. Zhang, Q. Lu, J. He, Z. Huo, R. Zhou, X. Han, M. Jia, C. Pan, Z.L. Wang, J. Zhai, Localizing strain via micro-cage structure for stretchable pressure sensor arrays with ultralow spatial crosstalk, Nat. Commun. 14 (2023) 1252, https://doi.org/10.1038/s41467-023-36885-3.

[6] H. Xu, W. Zheng, Y. Zhang, D. Zhao, L. Wang, Y. Zhao, W. Wang, Y. Yuan, J. Zhang, Z. Huo, Y. Wang, N. Zhao, Y. Qin, K. Liu, R. Xi, G. Chen, H. Zhang, C. Tang, J. Yan, Q. Ge, H. Cheng, Y. Lu, L. Gao, A fully integrated, standalone stretchable device platform with in-sensor adaptive machine learning for rehabilitation, Nat. Commun. 14 (2023), https://doi.org/10.1038/s41467-023-43664-7.

[7] L. Zu, J. Wen, S. Wang, M. Zhang, W. Sun, B. Chen, Z.L. Wang, Multiangle, self-powered sensor array for monitoring head impacts, Sci. Adv. 9 (2023) eadg5152, https://doi.org/10.1126/sciadv.adg5152.

[8] C.M. Boutry, M. Negre, M. Jorda, O. Vardoulis, A. Chortos, O. Khatib, Z. Bao, A hierarchically patterned, bioinspired e-skin able to detect the direction of applied pressure for robotics, Sci. Robot. 3 (2018) eaau6914, https://doi.org/10.1126/scirobotics.aau6914.

[9] D. Guo, S. Dong, Q. Wang, H. Yu, E.-S. Kim, Q. Xu, H.-K. Sung, Z. Yao, Y. Li, N.-Y. Kim, Enhanced sensitivity and detection range of a flexible pressure sensor utilizing a nano-cracked PVP hierarchical nanofiber membrane formed by BiI3 sublimation, Chem. Eng. J. 476 (2023) 146464, https://doi.org/10.1016/j.cej.2023.146464.

[10] G. Vauche, C. Corbier, Enhanced performance in energy of low frequency triboelectric-nanogenerator systems, J. Microelectromech. Syst. 33 (2024) 209–216, https://doi.org/10.1109/jmems.2023.3348872.

[11] C. Wan, P. Cai, X. Guo, M. Wang, N. Matsuhisa, L. Yang, Z. Lv, Y. Luo, X.J. Loh, X. Chen, An artificial sensory neuron with visual-haptic fusion, Nat. Commun. 11 (2020) 4602, https://doi.org/10.1038/s41467-020-18375-y.

[12] X. Wei, B. Wang, X. Cao, H. Zhou, Z. Wu, Z.L. Wang, Dual-sensory fusion self-powered triboelectric taste-sensing system towards effective and low-cost liquid identification, Nat. Food. 4 (2023) 721–732, https://doi.org/10.1038/s43016-023-00817-7.

[13] C. Wang, X. Zhang, J. Wu, X. Yu, T. Cheng, H. Ma, Z.L. Wang, Double-spring-piece structured triboelectric sensor for broadband vibration monitoring and warning, Mech. Syst. Signal Process. 166 (2022) 108429, https://doi.org/10.1016/j.ymssp.2021.108429.

[14] H. Tan, Y. Zhou, Q. Tao, J. Rosen, S. van Dijken, Bioinspired multisensory neural network with crossmodal integration and recognition, Nat. Commun. 12 (2021) 1120, https://doi.org/10.1038/s41467-021-21404-z.

[15] A. Gómez Eguíluz, I. Rañó, S.A. Coleman, T.M. McGinnity, Multimodal Material identification through recursive tactile sensing, Rob, Auton. Syst. 106 (2018) 130–139, https://doi.org/10.1016/j.robot.2018.05.003.

[16] H. Tang, Y. Yang, Z. Liu, W. Li, Y. Zhang, Y. Huang, T. Kang, Y. Yu, N. Li, Y. Tian, X. Liu, Y. Cheng, Z. Yin, X. Jiang, X. Chen, J. Zang, Injectable ultrasonic sensor for wireless monitoring of intracranial signals, Nature 630 (2024) 84–90, https://doi.org/10.1038/s41586-024-07334-y.

[17] Z. Song, J. Yin, Z. Wang, C. Lu, Z. Yang, Z. Zhao, Z. Lin, J. Wang, C. Wu, J. Cheng, Y. Dai, Y. Zi, S.-L. Huang, X. Chen, J. Song, G. Li, W. Ding, A flexible triboelectric tactile sensor for simultaneous material and texture recognition, Nano Energy 93 (2022) 106798, https://doi.org/10.1016/j.nanoen.2021.106798.

[18] Z. Zhao, Z. Quan, H. Tang, Q. Xu, H. Zhao, Z. Wang, Z. Song, S. Li, I. Dharmasena, C. Wu, W. Ding, A broad range triboelectric stiffness sensor for variable inclusions recognition, Nano-Micro Lett. 15 (2023) 233, https://doi.org/10.1007/s40820-023-01201-7.

[19] C. Dai, C. Ye, J. Ren, S. Yang, L. Cao, H. Yu, S. Liu, Z. Shao, J. Li, W. Chen, S. Ling, Humanoid ionotronic skin for smart object recognition and sorting, ACS Mater. Lett. 5 (2022) 189–201, https://doi.org/10.1021/acsmaterialslett.2c00783.

[20] P. Xu, J. Liu, X. Liu, X. Wang, J. Zheng, S. Wang, T. Chen, H. Wang, C. Wang, X. Fu, G. Xie, J. Tao, M. Xu, A bio-inspired and self-powered triboelectric tactile sensor for underwater vehicle perception, npj Flex Electron. 6 (2022), https://doi.org/10.1038/s41528-022-00160-0.

[21] J. Durrer, P. Agrawal, A. Ozgul, S.C.F. Neuhauss, N. Nama, D. Ahmed, A robot-assisted acoustofluidic end effector, Nat. Commun. 13 (2022) 6370, https://doi.org/10.1038/s41467-022-34167-y.

[22] Y. Wang, H. Wu, L. Xu, H. Zhang, Y. Yang, Z.L. Wang, Hierarchically patterned self-powered sensors for multifunctional tactile sensing, Sci. Adv. 6 (2020) eabb9083, https://doi.org/10.1126/sciadv.abb9083.

[23] J. Zhang, H. Yao, J. Mo, S. Chen, Y. Xie, S. Ma, R. Chen, T. Luo, W. Ling, L. Qin, Z. Wang, W. Zhou, Finger-inspired rigid-soft hybrid tactile sensor with superior sensitivity at high frequency, Nat. Commun. 13 (2022) 5076, https://doi.org/10.1038/s41467-022-32827-7.

[24] H. Zhang, H. Li, Y. Li, Biomimetic electronic skin for robots aiming at superior dynamic-static perception and material cognition based on triboelectric-piezoresistive effects, Nano Lett. 24 (2024) 4002–4011, https://doi.org/10.1021/acs.nanolett.4c00623.

[25] C. Zhao, J. Park, S.E. Root, Z. Bao, Skin-inspired soft bioelectronic materials, devices and systems, Nat. Rev. Bioeng. 2 (2024) 671–690, https://doi.org/10.1038/s44222-024-00194-1.

[26] X. Wei, B. Wang, Z. Wu, Z.L. Wang, An open-environment tactile sensing system: toward simple and efficient material identification, Adv. Mater. 34 (2022) e2203073, https://doi.org/10.1002/adma.202203073.

[27] S. He, J. Dai, D. Wan, S. Sun, X. Yang, X. Xia, Y. Zi, Biomimetic bimodal haptic perception using triboelectric effect, Sci. Adv. 10 (2024) eado6793, https://doi.org/10.1126/sciadv.ado6793.

[28] H. Qiao, S. Sun, P. Wu, Non-equilibrium-growing aesthetic ionic skin for fingertip-like strain-undisturbed tactile sensation and texture recognition, Adv. Mater. 35 (2023) e2300593, https://doi.org/10.1002/adma.202300593.

[29] S. Zhuo, Z. Zhao, Z. Xie, Y. Hao, Y. Xu, T. Zhao, H. Li, E.M. Knubben, L. Wen, L. Jiang, M. Liu, Complex multiphase organohydrogels with programmable mechanics toward adaptive soft-matter machines, Sci. Adv. 6 (2020) eaax1464, https://doi.org/10.1126/sciadv.aax1464.

[30] H. Niu, H. Li, S. Gao, Y. Li, X. Wei, Y. Chen, W. Yue, W. Zhou, G. Shen, Perception-to-cognition tactile sensing based on artificial-intelligence-motivated human full-skin bionic electronic skin, Adv. Mater. 34 (2022) e2202622, https://doi.org/10.1002/adma.202202622.

[31] X. Qu, Z. Liu, P. Tan, C. Wang, Y. Liu, H. Feng, D. Luo, Z. Li, Z.L. Wang, Artificial tactile perception smart finger for material identification based on triboelectric sensing, Sci. Adv. 8 (2022) eabq2521, https://doi.org/10.1126/sciadv.abq2521.

[32] T. Song, S. Jiang, N. Cai, G. Chen, A strategy for human safety monitoring in high-temperature environments by 3D-printed heat-resistant TENG sensors, Chem. Eng. J. 475 (2023) 146292, https://doi.org/10.1016/j.cej.2023.146292.

[33] H. Zhu, H. Luo, M. Cai, J. Song, A multifunctional flexible tactile sensor based on resistive effect for simultaneous sensing of pressure and temperature, Adv. Sci. 11 (2023) 2307693, https://doi.org/10.1002/advs.202307693.

[34] Y. Qiu, S. Sun, X. Wang, K. Shi, Z. Wang, X. Ma, W. Zhang, G. Bao, Y. Tian, Z. Zhang, H. Ding, H. Chai, A. Liu, H. Wu, Nondestructive identification of softness via bioinspired multisensory electronic skins integrated on a robotic hand, npj Flex Electron. 6 (2022), https://doi.org/10.1038/s41528-022-00181-9.

[35] U. Khan, T.H. Kim, H. Ryu, W. Seung, S.W. Kim, Graphene tribotronics for electronic skin and touch screen applications, Adv. Mater. 29 (2016) 1603544, https://doi.org/10.1002/adma.201603544.

[36] L. Xu, S. Zhong, T. Yue, Z. Zhang, X. Lu, Y. Lin, L. Li, Y. Tian, T. Jin, Q. Zhang, C. Lee, AIoT-enhanced health management system using soft and stretchable triboelectric sensors for human behavior monitoring, EcoMat 6 (2024) e12448, https://doi.org/10.1002/eom2.12448.

[37] G. Ye, Q. Wu, Y. Chen, X. Wang, Z. Xiang, J. Duan, Y. Wan, P. Yang, Bimodal coupling haptic perceptron for accurate contactless gesture perception and material identification, Adv. Fiber Mater. (2024) 1–13, https://doi.org/10.1007/s42765-024-00458-w.

[38] Y. Hao, J. Wen, X. Gao, D. Nan, J. Pan, Y. Yang, B. Chen, Z.L. Wang, Self-rebound cambered triboelectric nanogenerator array for self-powered sensing in kinematic analytics, ACS Nano 16 (2022) 1271–1279, https://doi.org/10.1021/acsnano.1c09096.

[39] B.D. Chen, W. Tang, C. He, C.R. Deng, L.J. Yang, L.P. Zhu, J. Chen, J.J. Shao, L. Liu, Z.L. Wang, Water wave energy harvesting and self-powered liquid-surface fluctuation sensing based on bionic-jellyfish triboelectric nanogenerator, Mater. Today. 21 (2018) 88–97, https://doi.org/10.1016/j.mattod.2017.10.006.

[40] Y. Zhou, X. Zhao, J. Xu, G. Chen, T. Tat, J. Li, J. Chen, A multimodal magnetoelastic artificial skin for underwater haptic sensing, Sci. Adv. 10 (2024) eadj8567, https://doi.org/10.1126/sciadv.adj8567.

[41] H. Zhu, J. Liang, S. Wang, J. Huang, Z. Chen, A multimodal PDMS triboelectric nanogenerator sensor based on anodised aluminium oxide template preparation for object recognition, J. Mater. Chem. A. 11 (2023) 24158–24168, https://doi.org/10.1039/d3ta04690g.

[42] G. Li, S. Liu, L. Wang, R. Zhu, Skin-inspired quadruple tactile sensors integrated on a robot hand enable object recognition, Sci. Robot. 5 (2020) eabc8134, https://doi.org/10.1126/scirobotics.abc8134.

[43] G. Kang, C.A.H. Allard, W.A. Valencia-Montoya, L. van Giesen, J.J. Kim, P. B. Kilian, X. Bai, N.W. Bellono, R.E. Hibbs, Sensory specializations drive octopus and squid behaviour, Nature 616 (2023) 378–383, https://doi.org/10.1038/s41586-023-05808-z.

[44] C. Chen, Z. Wen, J. Shi, X. Jian, P. Li, J.T.W. Yeow, X. Sun, Micro triboelectric ultrasonic device for acoustic energy transfer and signal communication, Nat. Commun. 11 (2020) 4143, https://doi.org/10.1038/s41467-020-17842-w.

[45] T. Chen, Q. Shi, M. Zhu, T. He, L. Sun, L. Yang, C. Lee, Triboelectric self-powered wearable flexible patch as 3D motion control interface for robotic manipulator, ACS Nano 12 (2018) 11561–11571, https://doi.org/10.1021/acsnano.8b06747.

[46] W. Li, C. Li, G. Zhang, L. Li, K. Huang, X. Gong, C. Zhang, A. Zheng, Y. Tang, Z. Wang, Q. Tong, W. Dong, S. Jiang, S. Zhang, Q. Wang, Molecular ferroelectric-based flexible sensors exhibiting supersensitivity and multimodal capability for detection, Adv. Mater. 33 (2021) 2104107, https://doi.org/10.1002/adma.202104107.

[47] M. Lou, I. Abdalla, M. Zhu, J. Yu, Z. Li, B. Ding, Hierarchically rough structured and self-powered pressure sensor textile for motion sensing and pulse monitoring,

ACS Appl. Mater. Inter. 12 (2019) 1597–1605, https://doi.org/10.1021/acsami.9b19238.

[48] D. Yang, H. Guo, X. Chen, L. Wang, P. Jiang, W. Zhang, L. Zhang, Z.L. Wang, A flexible and wide pressure range triboelectric sensor array for real-time pressure detection and distribution mapping, J. Mater. Chem. A. 8 (2020) 23827–23833, https://doi.org/10.1039/d0ta08223f.

[49] Z. Zhao, Q. Huang, C. Yan, Y. Liu, X. Zeng, X. Wei, Y. Hu, Z. Zheng, Machine-washable and breathable pressure sensors based on triboelectric nanogenerators enabled by textile technologies, Nano Energy 70 (2020) 104528, https://doi.org/10.1016/j.nanoen.2020.104528.